Faraday Discussions

Cite this: DOI: 10.1039/c7fd00200a

PAPER

View Article Online
View Journal

Published on 15 November 2017. Downloaded by INIST - CNRS on 01/02/2018 15:18:56.

Effect of point mutations on the ultrafast photo-isomerization of Anabaena sensory rhodopsin†

D. Agathangelou,[a] Y. Orozco-Gonzalez,[ag] M. del Carmen Marín,[b] P. P. Roy,[c] J. Brazard,[a] H. Kandori,[d] K.-H. Jung,[e] J. Léonard,[a] T. Buckup,[c] N. Ferré,[f] M. Olivucci[bgh] and S. Haacke*[a]

Received 27th September 2017, Accepted 13th November 2017
DOI: 10.1039/c7fd00200a

Anabaena sensory rhodopsin (ASR) is a particular microbial retinal protein for which light-adaptation leads to the ability to bind both the all-*trans*, 15-*anti* (AT) and the 13-*cis*, 15-*syn* (13C) isomers of the protonated Schiff base of retinal (PSBR). In the context of obtaining insight into the mechanisms by which retinal proteins catalyse the PSBR photo-isomerization reaction, ASR is a model system allowing to study, within the same protein, the protein–PSBR interactions for two different PSBR conformers at the same time. A detailed analysis of the vibrational spectra of AT and 13C, and their photo-products in wild-type ASR obtained through femtosecond (pump-) four-wave-mixing is reported for the first time, and compared to bacterio- and channelrhodopsin. As part of an extensive study of ASR mutants with blue-shifted absorption spectra, we present here a detailed computational analysis of the origin of the mutation-induced blue-shift of the absorption spectra, and identify electrostatic interactions as dominating steric effects that would entail a red-shift. The excited state lifetimes and isomerization reaction times (IRT) for the three mutants V112N, W76F, and L83Q are studied experimentally by femtosecond broadband transient absorption spectroscopy. Interestingly, in all three mutants, isomerization is accelerated for AT with respect to wild-type ASR, and this the more, the shorter the wavelength of maximum absorption. On the contrary, the 13C photo-reaction is slightly slowed down, leading to an

[a]*University of Strasbourg, CNRS, Inst. de Physique et Chimie des Matériaux de Strasbourg, 67034 Strasbourg, France. E-mail: haacke@unistra.fr*

[b]*Department of Biotechnology, Chemistry and Pharmacy, University of Siena, Via A. Moro 2, I-53100 Siena, Italy*

[c]*Physikalisch-Chemisches Institut, Ruprecht-Karls Universität Heidelberg, 69120 Heidelberg, Germany*

[d]*Department of Frontier Materials, Nagoya Institute of Technology, Showa-ku, Nagoya 466-8555, Japan*

[e]*Department of Life Science, Institute of Biological Interfaces, Sogang University, Shinsu-Dong 1, Mapo-Gu, Seoul 121-742, South Korea*

[f]*Aix-Marseille Univ., CNRS, ICR, Marseille, France*

[g]*Department of Chemistry, Bowling Green State University, Bowling Green, Ohio 43403, USA*

[h]*USIAS Institut d'Études Avanceés, University of Strasbourg, 67083 Strasbourg, France*

† Electronic supplementary information (ESI) available. See DOI: 10.1039/c7fd00200a

inversion of the ESLs of AT and 13C, with respect to wt-ASR, in the blue-most absorbing mutant L83Q. Possible mechanisms for these mutation effects, and their steric and electrostatic origins are discussed.

Published on 15 November 2017. Downloaded by INIST - CNRS on 01/02/2018 15:18:56.

Introduction

Light-induced processes in retinal proteins (RPs) have attracted vivid attention over the past two decades from experimentalists and theoreticians alike.[1–7] While initial work revealed the time scales for isomerization of the PSBR, and how they depend on the protein species or on point mutations, more attention was recently devoted to the mechanism, by which the protein steers this ultrafast reaction. New femtosecond spectroscopic[8–19] and quantum chemistry tools were devised[20–26] with the aim of drawing a very detailed picture of the excited state multi-dimensional potential energy surface (PES) including the conical intersection (CI) seam, of the time-resolved motion of PSBR at the atomic level, the reaction-driving vibrational modes and the dynamic changes in the charge distribution on PSBR and in the protein electrostatics. Additional, though partial, insight on these aspects comes from comparative studies of PSBR in solution[27–34] and of proteins reconstituted with non-isomerizing PSBR derivatives.[35–37]

While the relatively high complexity of the system impairs the ability to single out specific molecular or structural factors, it is generally accepted that the protein globally acts by limiting the isomerization to one specific double bond of the PSBR backbone and to increase the reaction quantum yield by steric and electrostatic constraints, preventing ultrafast non-productive routes[38] or possibly modifying the conical intersection (CI) topology.[22,39,40]

Nevertheless, the process by which the protein environment tunes the excited state PES or CI so as to shorten the S_1 lifetime and accelerate the reaction remains an open question. The recently discovered Anabaena Sensory Rhodopsin (ASR) offers a very interesting test ground in that context.[7,41–44] It bears a mixture of all-*trans*, 15-*anti* (AT) and 13-*cis*, 15-*syn* (13C) PSBR isomers, the relative content of which depends on the illumination, so-called 'light-adaptation' conditions. When left in the dark, the dark-adapted (DA) form adopts 97% AT, which drops to less than 40% under illumination with orange light, at neutral pH.[42,45] ASR therefore allows to study the PSBR protein interactions for two PSBR conformations, but with the same environment.

In this context, the observation of strikingly different excited state lifetimes (ESL) for AT (~0.7 ps (ref. 46 and 47)), and 13C (approx. 150 fs (ref. 44 and 47)) may be related to the different PSBR conformations,[48] but also to different electrostatic or dynamic interactions with the protein charge distribution. These findings were in qualitative agreement with quantum chemistry computations of the excited state PES along the minimum energy paths in ASR,[43] and with excited state trajectory calculations.[7] There, it was found that the S_1 PES of 13C is barrierless, while that of the AT form displays a plateau or a slight barrier that could account for a short resting period of the excited state population. Importantly, both reaction paths lead to a conical intersection seam with the ground state PES. The precise origin of these different shapes of the S_1 PES for both isomers remains unclear, however. As we reported recently,[48] a precise analysis of the nanosecond isomer difference spectra confirmed that AT has a 2.7 times higher reaction

 This journal is © The Royal Society of Chemistry 2018

Published on 15 November 2017. Downloaded by INIST - CNRS on 01/02/2018 15:18:56.

quantum yield (QY) than 13C, and that ASR has the lowest QY ever reported for RPs (<0.2). The former result is intuitively surprising, a shorter ESL would imply a larger QY,[49] but is related to the fact that both quantities are fundamentally independent since determined by separate, independent regions of the PES. While the ESL reports about population decay close to the Franck–Condon region, the QY is a matter of transition probabilities and wave packet trajectories around the CI.[47]

Here, we report on ultra-broadband probed transient absorption spectroscopy (TAS) and transient Raman experiments performed with <30 fs, respectively 20 fs time resolution. The latter reports new and precise data for the C=C, C–C stretch and methyl rocking frequencies for AT, 13C ground states and their primary photoproducts K_{AT} and K_{13C}. As an extension of previous reports on ASR wild-type, we are focussing here on the effect of point mutations on the ESL of AT and 13C isomers. The mutants investigated – V112N, L83Q and W76F – were chosen due to their high level of expression in *E. coli* and the relatively large blue shifts their DA and LA ground state spectra afford, indicating significant changes of the electrostatic protein–PSBR interactions with respect to wild-type. Structural details of the mutated PSBR environment are displayed in Fig. S0.† Interestingly, for AT, the blue shifts are correlated with a reduction of the ESL, attaining 120 fs for the blue-most shifted mutant L83Q. On the contrary, the ESL of 13C is barely affected or at most increased by a factor of two *via* mutations, as compared to wt-ASR.

Materials and methods

ASR mutants were expressed in *E. coli*, prepared according to reported protocols[24,31] and solubilized in buffer (150 mM NaCl, 50 mM Tris–HCL, 0.02% DDM, pH 7.0). Steady state absorption spectra of dark-adapted (DA) and light-adapted (LA) protein samples were obtained using a Perkin Elmer "Lambda 950" UV/vis spectrometer equipped with integrating sphere detection. DA samples were prepared by incubation in the dark for at least 12 h at room temperature. LA samples were obtained by constant illumination for 30 min using Luxeon LEDs, LXHL-NB98 (460 ± 15 nm), or LXHL-PL01 (590 ± 10 nm). The former is referred to as blue-adaptation (BA) and the latter as orange-adaptation (OA). The procedure for determining the absorption maxima of all-*trans*, 15-*anti* (AT) and 13-*cis*, 15-*syn* (13C) isomers was already described elsewhere.[47] We measure the absorption spectra of the DA and LA proteins, determine the isomer content in both states after retinal oxime extraction by high performance liquid chromatography (HPLC),[50] and use the fact that the absorption spectra of DA and LA are linear combinations of AT and 13C absorbances according to the equations:

$$\begin{bmatrix} \mathrm{AT} \\ \mathrm{13C} \end{bmatrix} = R^{-1} \times \begin{bmatrix} A_{\mathrm{DA}} \\ A_{\mathrm{LA}} \end{bmatrix} \text{ with } R = \begin{bmatrix} r_{\mathrm{DA}}^{\mathrm{AT}} & r_{\mathrm{DA}}^{\mathrm{13C}} \\ r_{\mathrm{LA}}^{\mathrm{AT}} & r_{\mathrm{LA}}^{\mathrm{13C}} \end{bmatrix} \quad (1)$$

TAS was carried out with an improved time resolution (IRF 40 ± 5 fs), using a home-built non-collinear OPA with typically 30 fs pulse width as a pump source. The spectral widths of the pulses were deliberately limited in order to reduce the spectral region of pump light scattering. The pump wavelength was adjusted to be

Published on 15 November 2017. Downloaded by INIST - CNRS on 01/02/2018 15:18:56.

on the low-energy side of the absorption maxima, *i.e.* 530 nm for L83Q, 535 nm for V112N, and 540 nm for W76F. The excitation density was kept low enough in order to be in a linear excitation regime. Broadband probing was achieved with white-light pulses (330–1000 nm) generated by 40 fs pulses at 800 nm in a 2 mm CaF_2 window. Acquisition of single TAS spectra on a 1 kHz rate, ensured high sensitivity ($\Delta A_{min} \approx 5 \times 10^{-5}$), which in the present case is rather limited by the scattering properties of the protein samples. Data are averaged from 14 time scans (1400 laser pulses). All data are corrected for signal contributions from the solvent or flow cell and for the white-light group velocity dispersion (20 fs accuracy).[47] All decay traces are fitted by multi-exponential functions convolved with the IRF approximated as a Gaussian.[51]

For the transient vibrational spectroscopy, DFWM and pump-DFWM experiments were employed as described in detail in ref. 52–54. In short, two home-built non-collinear optical parametric amplifiers (1 kHz) were used to generate ultrashort excitation and probing pulses with typical durations below 15 fs. The spectrum of actinic-pump (AP) was made resonant to the molecular ground state absorption, while the DFWM spectrum was spectrally overlapped with the photo-induced, ground state photo-product absorption of ASR, respectively (Fig. 3a and b). Energy of the AP beam was 100 nJ. DFWM energies were set to 50 nJ for the pump and Stokes and 10 nJ for the probe. A rapid scan measurement was realized with a piezo, which continuously scans the delay between Stokes and probe pulses (τ) (Fig. 3c). The delay between pump and Stokes (τ_{12}) was kept zero in all measurements. Vibrational spectra were obtained by Fourier transformation, zero padding and windowing the oscillatory signal after the initial 50 fs. The optical density (OD) of the ASR sample was around 0.9 at 545 nm. The sample was circulated through a fused silica flow cell with a path length of about 1 mm by a motor-driven pump.

Results and discussion

Effect of light- and dark-adaptation on steady-state absorption spectra of the mutants: experiments and computational results

The ground state absorption spectra of the LA and DA forms are reported in Fig. 1 for the 3 mutants studied and for wt-ASR as a reference (see Fig. S0† for positions of mutations). All DA spectra are normalized to 1.0, since extinction coefficients were not available, and the LA spectra are plotted with the experimental relative reduction in absorbance. Table 1 summarizes the wavelengths of absorption maxima, the isomer composition, as well as the absorption maxima of the isomer specific spectra (not shown) obtained after linear decomposition.[47] Light-adaptation was carried out either with an orange (OA) or a blue (BA) LED (see Materials and methods), and the light-adaptation with the highest 13C isomer ratio was retained. V112N and W76F exhibit a blue-shift under LA as wt-ASR and many other mutants. The absorption spectrum of the 13C isomer of these mutants shifts by 2 nm (V112N) and 8 nm (W76F). L83Q, the blue-most shifted mutant, surprisingly shows the opposite effect, with the 13C isomer being 6 nm red-shifted with respect to AT. Finally, we note that mutations induce 18, 21 and 33 nm blue-shifts, *i.e.* between 615 (76 meV) and 1160 cm^{-1} (145 meV) spectral shifts.

 This journal is © The Royal Society of Chemistry 2018

Published on 15 November 2017. Downloaded by INIST - CNRS on 01/02/2018 15:18:56.

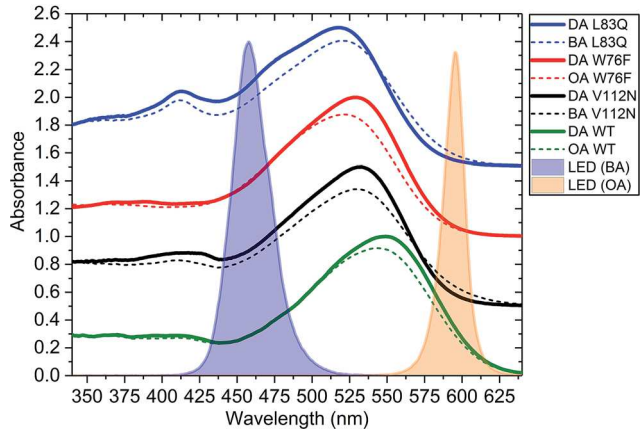

Fig. 1 Normalized ground state absorption spectra of light- and dark-adapted wt-ASR and the three mutants V112N, W76F and L83Q. Spectra are vertically shifted by multiples of 0.5 units. The spectral intensity distributions of the OA and BA LED's used for light-adaptation are displayed in orange and blue, respectively.

We report now the results obtained with QM/MM models of Anabaena Sensory Rhodopsin (ASR) and three of their mutants (V112N, W76F and L83Q) computed by the semi-automatic ARM protocol.[55] ARM employs the multi-configurational complete active space self-consistent field (CASSCF) method to obtain ground state geometries. Excitation energies are then computed using multi-configurational second-order perturbation theory (CASPT2) to recover the missing dynamical electron correlation associated with the CASSCF description.

Table 1 Isomer content of wt-ASR and the three mutants in the DA, OA and BA conditions, together with the measured maxima of absorption, highlighting the effect of light-adaptation. The maxima of isomer-specific ground state absorption spectra are calculated according to the linear decomposition method given in ref. 47

Sample	State	AT (%)	13C (%)	Abs max (nm)
WT	DA	97 ± 1	3 ± 1	550 ± 1
	OA	42 ± 1	58 ± 1	543 ± 1
	AT			550 ± 1
	13C			537 ± 1
V112N	DA	98 ± 1	2 ± 1	532 ± 1
	BA	42 ± 1	58 ± 1	530 ± 1
	AT			532 ± 1
	13C			527 ± 1
W76F	DA	96 ± 1	4 ± 1	529 ± 1
	OA	42 ± 1	58 ± 1	521 ± 1
	AT			529 ± 1
	13C			514 ± 1
L83Q	DA	98 ± 1	2 ± 1	517 ± 1
	BA	44 ± 1	56 ± 1	520 ± 1
	AT			517 ± 1
	13C			523 ± 1

Published on 15 November 2017. Downloaded by INIST - CNRS on 01/02/2018 15:18:56.

The computed values obtained with ARM, are reported in Table S1 (*cf.* ESI†) and plotted in Fig. 2, where they are compared to the experimental values determined above. Apart from the previously documented[55] $\approx$2–3 kcal mol^{-1} overestimation of the computed values, the experimental trend is well reproduced for all mutants except for L83Q, where the ARM model fails to reproduce the observed λ_{max} values, and predicts the opposite trend of LA. Further investigation reveals that the discrepancy with respect to experiments is related to the orientation of the O–H dipole moment of the Glu83 residue towards the protonated Schiff base nitrogen (see Fig. S2 in ESI†). The QM/MM model generated by the ARM protocol orients this dipole with the positive end facing the SB (Fig. S2A†), leading to destabilization of the ground state (S_0). However, a second lower energy minimum (see Table S2 in the ESI†) is found, manually, for an orientation of the O–H dipole, with the negative end pointing toward the SB nitrogen (see Fig. S2B†), thus stabilizing S_0, and generating a blue-shift of λ_{max} similar to the experimental value. Nevertheless, while the L83Q$^*_{AT}$ appears to provide a λ_{max} substantially in line with the general trend, L83Q$^*_{13C}$ is clearly too blue shifted and, thus, the LA effect is not predicted in the right order (see also Table S1†). Within a new computational protocol analyzing the total free energy of the protein,[82] we are presently exploring a possible isomer-dependence of the protonation states of other amino acids in the retinal binding pocket, and orientation of Glu83 and Lys. We conclude that LA, in L83Q, causes a structural modification that cannot be correctly captured by the present modelling technique. Accordingly, the L83Q computational data will not be discussed/analyzed in the following.

We now focus on the differences between the WT model and the V112N and W76F mutant models. Mutants are usually challenging to model due to the smaller changes in the observed $\Delta E_{S_1-S_0}$ values and the absence of crystallographic data or other structural information. In spite of this difficulty, the computed WT, V112N and W76F $\Delta E_{S_1-S_0}$ trend parallels the observed values with only a relatively

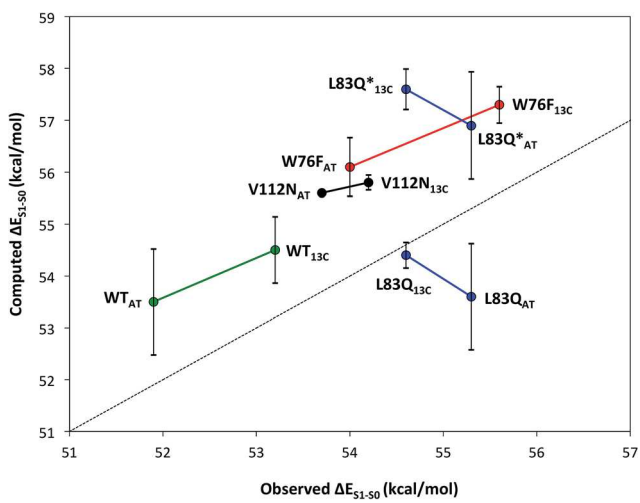

Fig. 2 Comparison between computed and observed $\Delta E_{S_1-S_0}$ (kcal mol^{-1}) values from ARM models of ASR WT (green), V112N (black), W76F (red), L83Q and modified L83Q* (blue) mutants. The error bars of the standard deviation are shown in black.

 This journal is © The Royal Society of Chemistry 2018

Published on 15 November 2017. Downloaded by INIST - CNRS on 01/02/2018 15:18:56.

small blue-shifted deviation in the absolute $\Delta E_{S_1-S_0}$ values. The mutants studied show significant blue-shifts with respect to the WT reference, *e.g.* the computed $\Delta E_{S_1-S_0}$ change between WT and the most blue-shifted mutant (W76F) is 2.6 kcal mol^{-1} for the AT and 2.8 kcal mol^{-1} for the 13C isomer. We have computationally disentangled the electrostatic and steric effects causing the total blue shift by computing the $\Delta E_{S_1-S_0}$ values of the three chromophores in the gas-phase (keeping the chromophore geometries fixed at their optimized protein structure). In fact, the gas-phase $\Delta E_{S_1-S_0}$ value reflects the change in chromophore geometry induced by only the steric interaction with the protein cavity. By comparing the electrostatic and steric effects of the different chromophore cavities, we show that the electrostatic effect is the dominant one (Table 2, last column). These effects are due to the different stabilization of the chromophore ground state (S_0) and first excited state (S_1), which are characterized by different electronic distributions (Fig. S1†), due to the change in the protein charges and positions induced by the mutation. It is well-known that PSBR's photo-excited state S_1 is characterized by a partial charge transfer (*ca.* 30%)[56] electronic configuration. On the other hand, S_0 is dominated by a covalent electronic configuration, with the positive charge localized at the protonated Schiff base. The interaction of both electronic configurations with the mutated PSBR binding cavity explains the observed blue-shifts: for both the V112N and W76F mutants, a change from valine and tryptophan to asparagine and phenylalanine respectively, near the β-ionone ring of the chromophore produces a destabilization of the S_1 rather than a stabilization of S_0. The observed blue-shift is thus a combined effect of S_1 up-shift and S_0 down-shift, but the former is larger in amplitude than the latter, which may be important information for the mutation effects on the S_1 kinetics (see Table S3 in the ESI†).

Notice that, as usually found,[57] the chromophores separated from their protein environments present $\Delta E_{S_1-S_0}$ values about 12–20 kcal mol^{-1} ($\Delta E_{S_1-S_0}$ vacuum) lower than for the chromophore inside the protein ($\Delta E_{S_1-S_0}$ protein environment) (Table 2). Interestingly, the mutation-induced changes of the PSBR configurations cause, with respect to the WT, a red-shift and not a blue-shift in all $\Delta E_{S_1-S_0}$ values. However, as is shown in Table 2, the electrostatic contribution of the cavity dominates, causing a global blue-shift for the present mutants, with the strongest

Table 2 Comparison of the vertical excitation energies $\Delta E_{S_1-S_0}$ (kcal mol^{-1}) computed at the CASPT2/CASSCF(12,12)/6-31G*/AMBER level of theory for ASR WT and the mutants V112N and W76F when the retinal chromophore is inside the protein ($\Delta E_{S_1-S_0}$ protein environment) and in vacuum ($\Delta E_{S_1-S_0}$ vacuum), supposing the same conformation as in the protein. This allows to separate the dominant electrostatic effect of the mutations from conformational changes

Sample	State	$\Delta E_{S_1-S_0}$ protein environment	$\Delta E_{S_1-S_0}$ vacuum (steric contribution)	Effect of mutation: e.-static contribution
WT	AT	53.5	41.8	
	13C	54.5	43.1	
V112N	AT	55.6	40.2 (−1.6)	+3.7
	13C	55.8	40.9 (−2.2)	+3.5
W76F	AT	56.1	36.3 (−5.5)	+8.1
	13C	57.3	39.1 (−4.0)	+6.8

Published on 15 November 2017. Downloaded by INIST - CNRS on 01/02/2018 15:18:56.

effect observed for the W76F mutant. In conclusion, the observed blue-shifts of the V112N and W76F are dominated by the change in the electrostatics of the chromophore hosting cavity. In Fig. S3† we provide a qualitative explanation of the electrostatic effects, which clearly show how the V112N mutation creates a new dipole moment destabilizing S_1 with respect to S_0. In contrast, the W76F mutation removes a dipole moment vector, which, in wild-type, stabilizes the S_1 with respect to S_0.

Photo-isomerization kinetics of wild-type ASR studied by femtosecond vibrational spectroscopy

Understanding the ultrafast vibrational evolution is a central aspect in the investigation of the reaction dynamics of the retinal chromophore.[58–63] Time resolved vibrational spectroscopies, like degenerate four wave mixing (DFWM),[53,64] pump-degenerate four wave mixing (pump-DFWM),[52,54,65–69] impulsive vibrational spectroscopy (IVS),[67,70–74] or femtosecond stimulated Raman (FSRS),[75,76] allow to resolve such structural changes in the ground and electronically excited states up to the formation of photoproducts. A detailed study of the evolution and origin of vibrational modes in the ground and excited state has been done, for example, in the case of bacteriorhodopsin (bR).[53,64,74] Excitation of vibrational coherences in bR has been shown to be highly dependent on the excitation wavelength in the spectral range from 520 up to 620 nm.[53] The "out-of-plane" modes of polyene-chain substituents and low frequency modes have been found to be very intense in the electronically excited state of bR. Contrasting to that, all remaining experimentally observed high frequency modes above 1010 cm^{-1} have to be assigned to the ground state manifold. A similar picture has been also observed for all-*trans*-retinal protonated Schiff-bases (RPSB).[64] While the origin of the experimental vibrational spectra and the vibrational dynamics of other retinal based systems, like bR and RPSB, has been already established, very little is known for ASR. In particular, it is still unknown how the retinal isomerization and environment alters the topology of PES and hence vibrational dynamics.[77] In this section, non-resonant DFWM and pump-DFWM (Fig. 3) is applied to DA and LA ASR. In particular, all the high frequency modes (>800 cm^{-1}) of ground states and photoproducts were compared both in DA and LA conditions.

Electronic ground state of AT and 13C. Non-resonant DFWM transients detected at 610 nm in DA and LA conditions display strong high frequency oscillations (Fig. 4a and b). The respective FFT spectra show characteristic localized high frequency vibrational modes: DA ASR shows four main peaks at 1003, 1165, 1230 and 1530 cm^{-1}; LA ASR shows only three major peaks at 1007, 1180 and 1539 cm^{-1} and a smaller one at 1300 cm^{-1}. The mode at about 1003/1007 cm^{-1} is assigned to the CH_3 rocking, while the mode at 1530/1539 cm^{-1} is assigned to the C=C stretching.[53,64–66] The blue shift of the frequency of the C=C stretching mode and the CH_3-rocking mode (smaller shift) due to light adaptation agrees with previous experimental observations.[74] The modes at 1165 and 1230 cm^{-1} observed for the DA ASR are characteristic for the C–C single bond stretch of the AT retinal isomer. For bR, these two frequencies are at 1165 cm^{-1} and 1210 cm^{-1}. The respective C–C mode for the LA ASR is at 1180 cm^{-1}. In bR, this mode is at 1190 cm^{-1} and is commonly attributed to the formation of the 13C isomer.[78]

 This journal is © The Royal Society of Chemistry 2018

Published on 15 November 2017. Downloaded by INIST - CNRS on 01/02/2018 15:18:56.

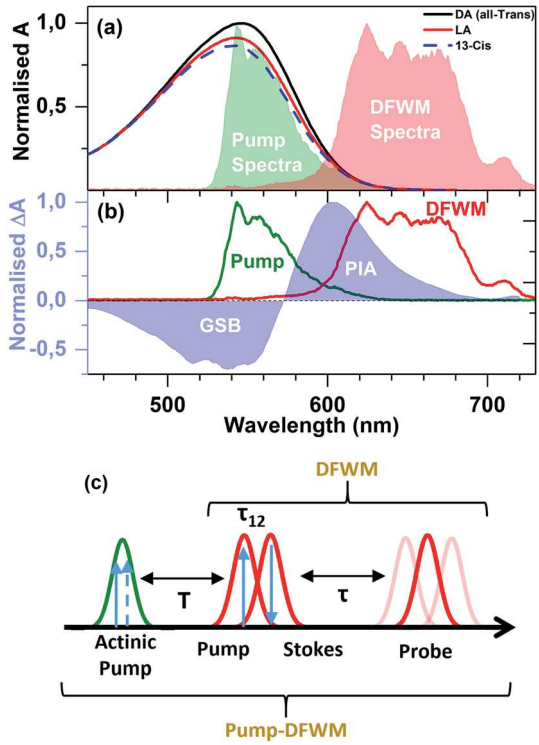

Fig. 3 (a) Ground state absorption spectra of ASR in DA and LA conditions. (b) Normalized difference absorption spectra at a pump-probe delay of 100 ps. Green and red (solid in (a) and line in (b)) curves represent the spectrum of AP and degenerate P. (c) Schematic of the pulse sequence and definition of the relevant delay times.

The contributions of each isomer to the DA and LA signals can be separated by fitting the individual FFT spectra with Gaussian line shapes and considering the isomer content in each case. Since DA ASR contains almost pure-AT isomer, a fitting of the respective FFT spectra delivers the pure vibrational frequencies

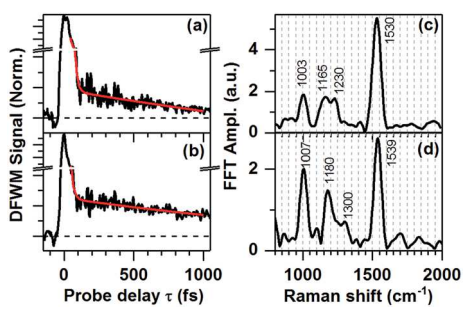

Fig. 4 Non-resonant DFWM transients probed at 610 nm: (a) DA ASR, (b) LA ASR. (c) FFT spectra of oscillatory signal of (a). (d) FFT spectra of oscillatory signal of (b). Non-oscillatory contribution (red line) was fitted by exponential decay and subtracted before FFT.

Published on 15 November 2017. Downloaded by INIST - CNRS on 01/02/2018 15:18:56.

and widths of AT ground state modes. This information can be used to disentangle the pure-13C spectra by using a constrained double Gaussian fit for LA ASR, here orange-adapted, which contains both AT and 13C isomers. This is illustrated for the C=C stretching mode (Fig. 5a). In this case, the centre frequency and width of one Gaussian was fixed to the value obtained by single Gaussian fitting of DA ASR (=AT) (see Table S3 in the ESI† for fitting parameters). As the second Gaussian basically represents only the signature of 13C, the pure contribution of 13C can be retrieved by using HPLC isomeric ratio (58% 13C + 42% AT, Table 1). A comparison of AT and reconstructed-13C spectra shows that the C=C line shape is narrower and lower in amplitude. A similar approach can also be applied to the CH_3 rocking mode to separate the AT and 13C-isomeric contributions (see ESI†). The frequency difference of this mode for AT and 13C is about 5 cm^{-1}, while the widths are comparable within the fitting error. Separation of the isomeric contribution to the peaks in the fingerprint region 1100–1400 cm^{-1} is more challenging due to the strong spectral overlap between Raman lines and will be presented elsewhere.

The different Gaussian widths obtained for the 13C (52 cm^{-1}) and AT (68 cm^{-1}) above suggests that the C=C mode undergoes different dephasing dynamics for each isomer, *i.e.* the C=C mode for the 13C isomer dephases much slower than for AT. This can be further corroborated by directly comparing the dephasing rates *via* a sliding window FFT along several probe delays τ.[53] Fig. 5b compares the decay of the amplitude of the C=C mode obtained this way for the AT (=DA GS) and 13C (retrieved from LA data). While the C=C stretching dephases with a lifetime of about 750 fs in the AT GS, the same mode in the ground state of the 13C GS dephases slower with a time constant of 1030 fs. Moreover, since the LA form contains both AT and 13C, a constrained bi-exponential fitting reproduces the LA spectra well by fixing the time constants

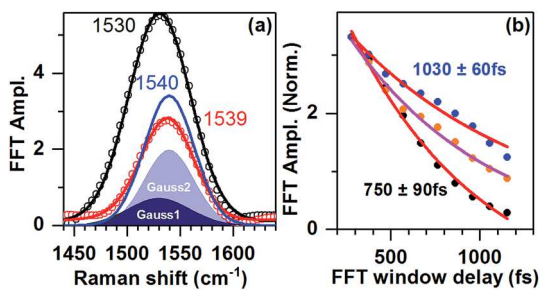

Fig. 5 (a) Gaussian fit of C=C stretching mode of GS ASR in DA (black curve) and LA (red curve) conditions. The DA GS peak was fitted with a single Gaussian. For LA GS, a double Gaussian constrained fit was performed fixing the centre and width of first Gaussian (Gauss1) as obtained by fitting the DA GS. The Gaussians required to fit the LA GS line shape are shown as filled curves. The reconstructed pure-13C spectrum is represented as a blue line. (b) Exponential fit of dephasing of GS C=C stretching mode obtained by sliding window FFT. Dephasing of DA (=AT), LA and extracted 13C isomer are shown by black, orange and blue dots. Red and pink solid lines represent the exponential and constrained bi-exponential fitting, respectively.

 This journal is © The Royal Society of Chemistry 2018

Published on 15 November 2017. Downloaded by INIST - CNRS on 01/02/2018 15:18:56.

(750 fs and 1030 fs) obtained for AT and 13C, but keeping the amplitudes free (Fig. 5b).

K photoproducts. In order to compare the K photoproduct's vibrational signature with the electronic ground state of each isomer (see above), a pump-DFWM experiment was carried out. A resonant AP pulse was used to initiate the isomerization reaction. The DFWM pulse sequence, which was set spectrally resonant to the photoproduct absorption, was delayed by $T = 100$ ps. At this delay, the isomerization of C_{13}=C_{14} is completed and a vibrationally relaxed K-photoproduct is already obtained.[60,61] The pump-DFWM signal measured shows similar vibrations as DFWM but with slightly shifted frequencies. FFT spectra of respective transients show for DA ASR four peaks at 1003, 1170, 1245 and 1535 cm^{-1}, while for LA ASR the peak frequencies are at 1007, 1174, 1305 and 1532 cm^{-1} (Fig. 6). Table 2 in the ESI† compares all values for the ground states of DA, LA and at $T = 100$ ps.

Discussion. Comparison of the FFT spectra obtained for the ground state of AT and 13C isomers and the respective photoproducts shows three major features regarding frequency shifts. The first one is the blue shift of the C=C stretching band (1530 to 1535 cm^{-1}) from GS to $T = 100$ ps in DA conditions, whereas it gets red shifted (1539 to 1532 cm^{-1}) in LA conditions (Fig. 4 and Table S4 in the ESI†). These differences can be rationalized by the structural differences at the C_{13} and C_{15} double bonds for the ground states and the respective photoproducts. For the two isomers in the ground state, both double bonds are *trans* (AT) or *cis* (13C) isomerized, which results in a 10 cm^{-1} blue shift for this mode (Fig. 3a). For the photoproducts, K_{AT} and K_{13C}, one of the two double bonds is in *trans*- while the other is in *cis*-conformation. In this situation one expects a frequency for this mode between 1530 cm^{-1} (AT) and 1540 m^{-1} (13C). Moreover, since at $T = 100$ ps the signal contains contributions of ground states as well as from the respective photoproducts, the frequency of C=C stretching appears at a frequency between the frequency of the AT and 13C, *i.e.*, at 1535 cm^{-1} in DA and 1532 cm^{-1} in LA conditions. The second aspect is the absence of any shift for the CH_3-rocking mode when the ground state is compared to the respective photoproduct (Table S4 in the ESI†). For example, for DA ground state as well as at $T = 100$ ps the frequency is 1003 cm^{-1}. This contrasts with the frequency shift observed for the ground states of AT (1003 cm^{-1}) and 13C (1007 cm^{-1}), and suggests that the CH_3

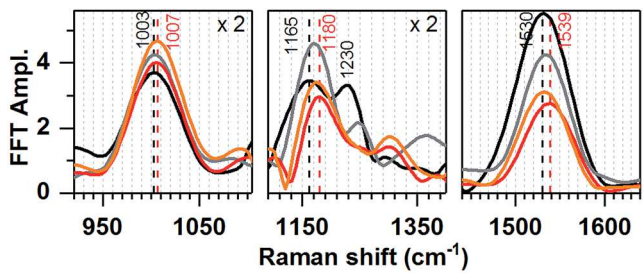

Fig. 6 Comparison of FFT spectra of DA and LA ASR for different vibrational modes. Black and red curves show FFT spectra of ground states of ASR in DA and LA conditions. Grey and orange curves represent the FFT spectra obtained from pump-DFWM transient at $T =$ 100 ps for DA and LA conditions, respectively.

Published on 15 November 2017. Downloaded by INIST - CNRS on 01/02/2018 15:18:56.

rocking mode is more sensitive when isomerization at both C_{13}- and C_{15}-positions takes place. The last and more complex aspect of the frequency shifts observed is in the fingerprint region between 1100 and 1400 cm^{-1}. Although many vibrational modes are overlapping in this region, large changes in frequency from GS to $T =$ 100 ps are quite evident. Similar to the C=C stretching mode, the 1165 cm^{-1} mode blue shifts to 1170 cm^{-1} for DA ASR, whereas in LA conditions 1180 cm^{-1} red shifts to 1174 cm^{-1}. In addition, a band at 1230 cm^{-1} observed for DA GS is reduced at $T = 100$ ps. This band vanishes for LA ASR whereas a new peak around 1300 cm^{-1} appears. It is very similar to the 13C isomer of bR[79,80] and Channelrhodopsin,[73] where it has been assigned to CH_3 rocking and marked as a signature of *cis*-configuration.

Effects of point mutations on the photo-reaction kinetics of all-*trans*, 15-*anti* PSBR

The reaction kinetics of the all-*trans* species are retrieved from TAS data measured on DA mutants, as described in the Materials and methods section. Fig. 7 reports the time-resolved TAS spectra for W76F and L83Q, at time delays between 40 fs and 1.0 ps, and long-time difference spectra (90 ps) representing the AT-K_{AT} difference spectra.

Until 100–150 fs, the spectra show a prominent excited state absorption (ESA) in the range from 420 to 620 nm, and stimulated emission (SE) beyond 630 nm. During this early time period, significant dynamic spectral shifts are observed redistributing the ESA spectral intensity to shorter wavelengths, and allowing for the ground state bleach (GSB) to show up progressively as a trough in the ESA (L83Q-AT) or a negative signal (W76F-AT). This is most obvious for L83Q-AT, where the ESA maximum shifts from 550 to 540 nm within 60 fs. This initial phase of relaxation (<0.1 ps) is attributed to excited state relaxation, most likely due to C=C bond length alternation and IVR. GSB is observed at all delay times at wavelengths shorter than 400 nm.

After 100 fs, the ESA and SE globally decay in amplitude, indicating excited state decay due to isomerization. In contrast, the spectral range between 570 and 670 nm, now displays an increasing differential absorption, consistent with the

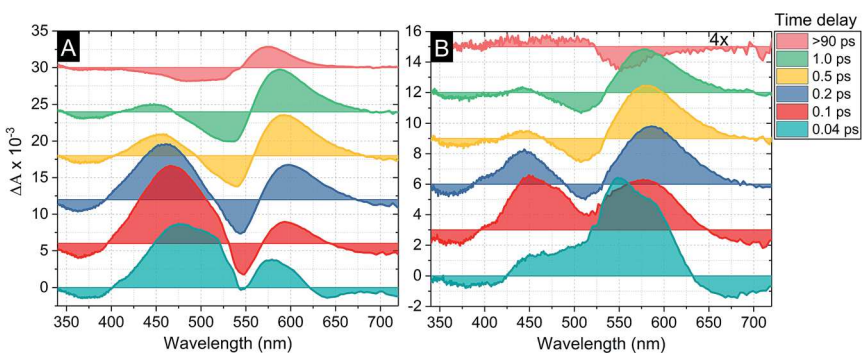

Fig. 7 Time-resolved TAS spectra for the AT forms of W76F (A) and L83Q (B) for highlighting delays up to 1.0 ps and a long-time, 90 ps, GS-K difference spectrum. Note the prominent spectral shifts of ESA, GSB and SE in the first 200 fs.

 This journal is © The Royal Society of Chemistry 2018

Published on 15 November 2017. Downloaded by INIST - CNRS on 01/02/2018 15:18:56.

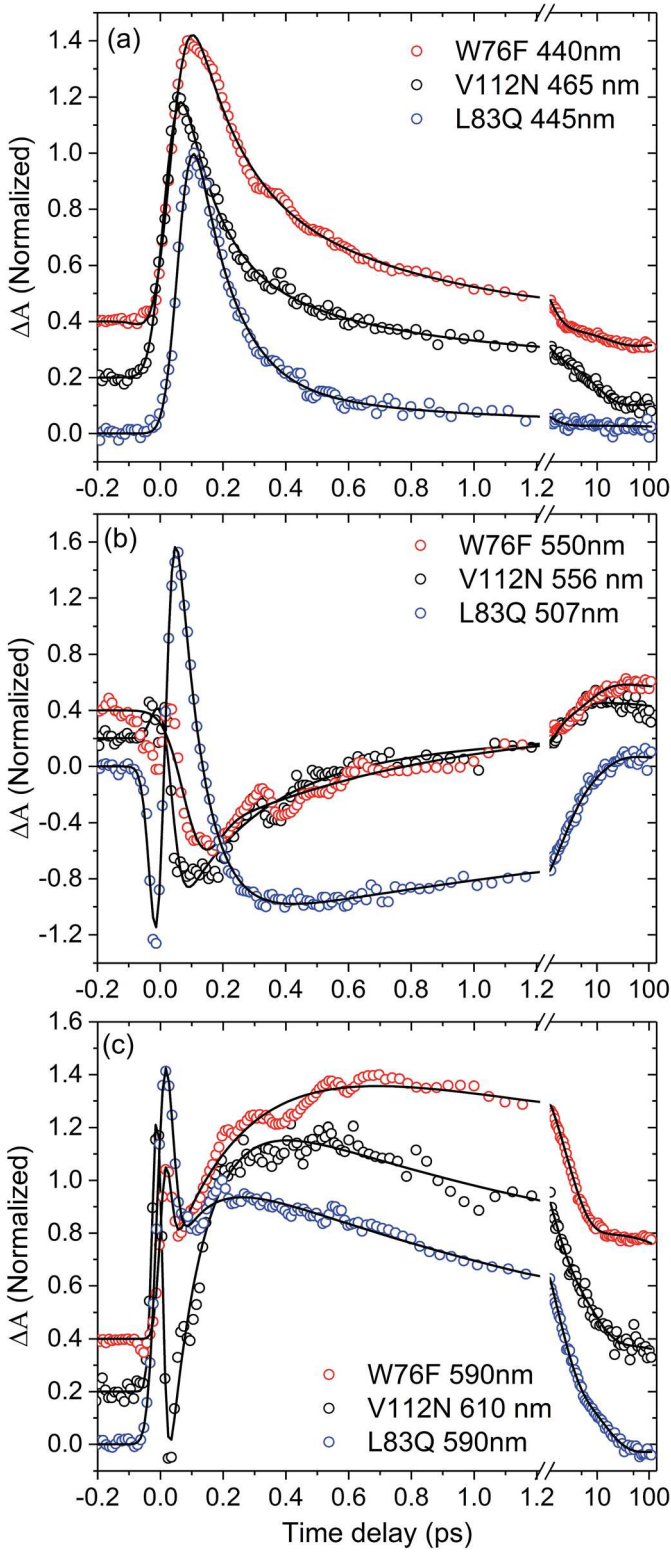

Published on 15 November 2017. Downloaded by INIST - CNRS on 01/02/2018 15:18:56.

Table 3 Isomerization reaction times for AT and 13C isomers in the 3 mutants studied. Times are determined from ESA decay, PP rise and GSB recovery times. A2 ≠ 0 refers to bi-phasic excited state population decay. See text for details

Sample	Isomer	A_1	τ_1 (fs)	A_2	τ_2 (fs)	IRT (fs)
W76F	AT	0.67	140 ± 10	0.33	700 ± 30	340 ± 40
	13C	1.0	120 ± 30			120 ± 30
V112N	AT	0.72	110 ± 10	0.28	490 ± 80	230 ± 20
	13C	1.0	290 ± 50			290 ± 50
L83Q	AT	1.0	120 ± 30			120 ± 30
	13C	1.0	200 ± 40			200 ± 40

formation of the J_{AT} photo-product, as reported for wt-ASR.[44,47] The high-energy part of ESA, 400–500 nm, continues decaying and slightly blue-shifting until 1.0 ps. It is not clear, whether the remaining amplitude at 430–450 nm is ESA or part of the GS-J_{AT} difference spectrum, slowly decaying on a ps timescale (see below).

The spectral overlap of ESA and J_{AT}, throughout the entire 420–620 nm range, requires a careful analysis of the TAS transients for the determination of the excited state lifetime (ESL) and isomerisation reaction time (IRT). The SE decay reflects the ESL on a zero background and is therefore of particular relevance (see below). In addition, ESL and IRT have to be consistent with the PP rise time.

For L83Q, the ESA decay in the blue part of the spectrum after the initial 100 fs spectral shift can be fitted at 445 nm with a bi-exponential decay, featuring a dominant 120 ± 10 fs component and a 10-times smaller 0.76 ± 0.13 ps component (Fig. 8a). For shorter wavelengths, where the J absorption is negligible (424 nm, not shown) the slower component vanishes. The SE decay at >700 nm is purely mono-exponential with a 110 ± 10 fs decay (see ESI, Fig. S5†) indicating clearly that the S_1 population decays on this ultrafast timescale, *i.e.* 7 times faster than AT in wt-ASR.[47] This is corroborated by the 110 ± 10 fs risetime of the J_{AT} PP absorption followed by a 1.54 ± 0.06 ps decay due to $J_{AT} \rightarrow K_{AT}$ relaxation (Fig. 8c). The GSB in the 507 nm trace sets in only after the initial ESA decay and cannot inform about the isomerization-related GS recovery (Fig. 8b). Nevertheless, from the ESA, SE and PP kinetics it is clear that the IRT for L83Q-AT is 110 ± 10 fs.

For W76F, the ESA decay at 440 nm shows a bi-exponential decay with a dominant 140 ± 10 fs component and a 2.0 times smaller 0.70 ± 0.03 ps component (Fig. 8a). The slower component is present also in ESA traces at shorter wavelengths where the J contribution is smaller (*e.g.* 415 nm, not shown) even with a smaller amplitude. The SE at >700 nm does not afford a high SNR (see ESI, Fig. S5†), but a mono-exponential fit yields an excited state lifetime of 360 ± 20 fs, in good agreement with a weighted average of the above ESA components. We thus conclude that for W76F the S1 decay is biphasic. In the PA trace at 590 nm (Fig. 8c), only a fast 240 ± 20 fs rise component is observed, followed by a slower 2.55 ps $J_{AT} \rightarrow K_{AT}$ relaxation decay. The GSB recovery displays significant

Fig. 8 Normalized kinetic traces of the AT isomer in the 3 mutants, and probed at the wavelengths indicated. (a) ESA decay, (b) GSB recovery, (c) PP formation. Solid lines represent fits, according to the parameters discussed in the text. The W76F and V112N traces are displaced vertically.

 This journal is © The Royal Society of Chemistry 2018

Published on 15 November 2017. Downloaded by INIST - CNRS on 01/02/2018 15:18:56.

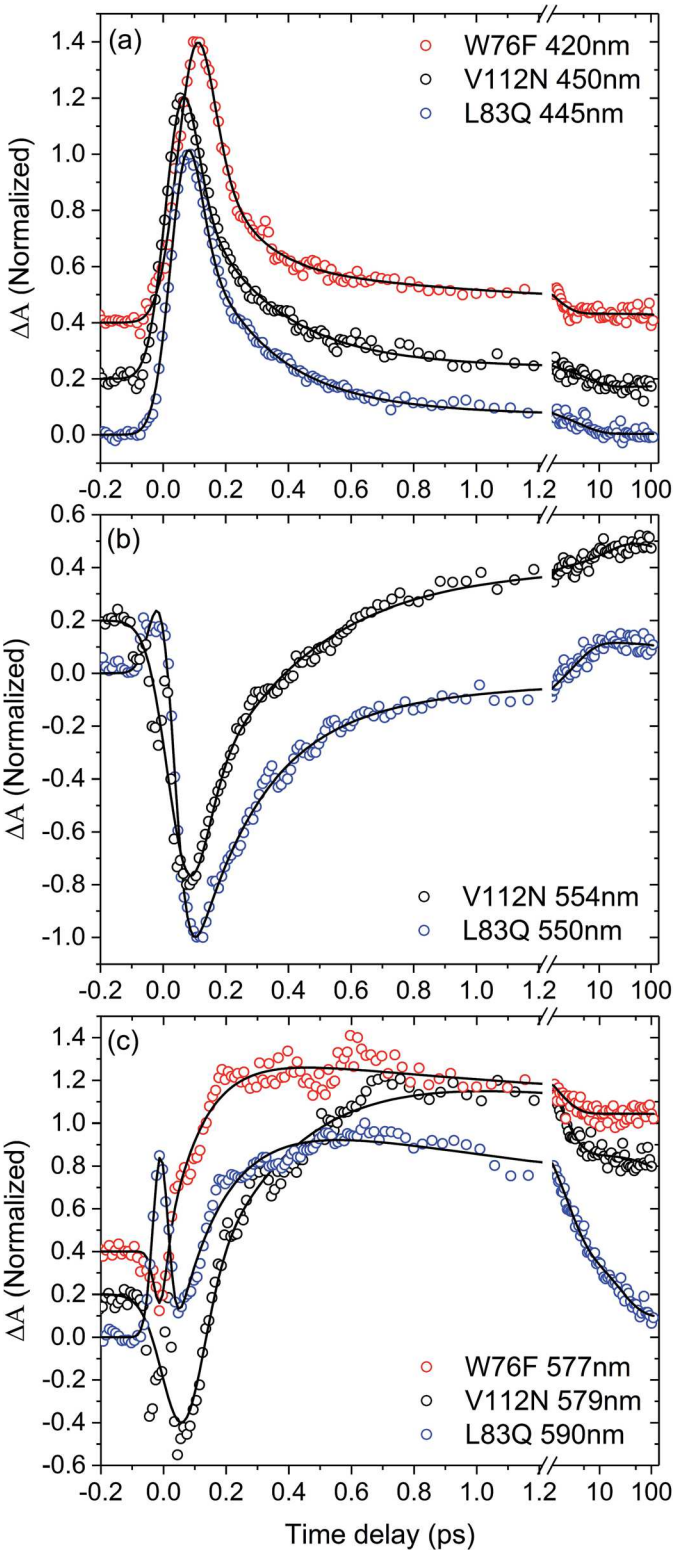

Published on 15 November 2017. Downloaded by INIST - CNRS on 01/02/2018 15:18:56.

non-exponential features (Fig. 8b), but the non-oscillating part is consistent with the above biphasic isomerization reaction (Table 3).

The situation is not as clear for V112N. Here, the ESA decay is bi-exponential with a dominant 110 ± 10 fs component and a 2.6-times smaller 490 ± 80 fs. SE is weaker at >700 nm than for the other mutants (see ESI, Fig. S5†), and shows a dominant 110 ± 10 fs component. The existence of a slower decay component cannot be excluded but is hidden in the noise floor. The PP rise is clearly faster than for V112N and shows only the fastest 110 ± 10 fs rise component followed by a slower 1.1 ps decay due to $J_{AT} \rightarrow K_{AT}$ relaxation decay (Fig. 8b). The GSB recovery, at 556 nm, also displaying oscillatory features as the PP kinetics, can be best fitted by a fast 250 ± 30 fs component, indicating that the isomerization is not completed on a 110 fs timescale, but that the IRT is most likely composed of the above two 110 and 490 fs components. A weighted average gives 210 fs. We retain 230 ± 20 fs for the IRT (see Table 3).

In summary, we find IRT's from 110 to 340 fs for the three mutants, which are 2 to 7 times shorter than the one for wt-ASR. We note that the blue-shift of the ground state absorption of AT correlates with a shorter IRT, with respect to wt-ASR. Notably, a similar correlation, though with less amplitude in the IRTs, was predicted theoretically by comparing different RPs.[81]

Effects of point mutations on the photo-reaction kinetics of 13-*cis*, 15-*syn* PSBR

The 13C-specific TAS kinetics are extracted from the LA data following the decomposition procedure used in ref. 47. Here we take into account the ground state isomer composition determined by HPLC under exactly the same LA conditions, and the excited state isomer composition calculated from the pump laser spectrum and the relative absorption amplitudes of AT and 13C (Fig. 1).

The effects of the mutations on the ESL and IRT are evaluated from selected ESA, GSB and PP kinetics. SE kinetics are not available with high enough signal-to-noise ratio for the 13C isomers. The time-resolved spectra are qualitatively equivalent to the ones observed for AT (Fig. 7), and will not be shown here. Fig. 9 displays the relevant kinetics for the 3 mutants. The longest ESL is observed for V112N (240 ± 30 fs) in the ESA, which displays an additional 5.7 ps decay time, 12 times smaller in amplitude, most probably due to a longer-lived signal assigned to the J_{13C} intermediate. The PP rise and GSB recovery times are 310 and 340 fs, respectively. Taken together, the IRT is 290 ± 50 fs for this mutant, *i.e.* twice as long as for wt-ASR.

For L83Q, the IRT of 13C is slightly longer than in wt-13C. We find 200 ± 40 fs, as a combination of ESA decay (220 fs), PP rise (160 fs) and GSB recovery (220 fs). ESA shows an additional 8-times smaller 4.3 ps decay component, which is attributed again to the J_{13C} intermediate. The 13C reaction kinetics in W76F do not seem to be affected by the mutations, since it is found to be 120 ± 30 fs, as a result of ESA decay (120 ± 30 fs, 8 times larger amplitude than a spurious 1.5 ps component) and PP rise (110 ± 10 fs).

Fig. 9 Normalized kinetic traces of the 13C isomer in the 3 mutants, and probed at the wavelengths indicated. (a) ESA decay, (b) GSB recovery, (c) PP formation. Solid lines represent fits, according to the parameters discussed in the text. The W76F and V112N traces are displaced vertically.

 This journal is © The Royal Society of Chemistry 2018

Published on 15 November 2017. Downloaded by INIST - CNRS on 01/02/2018 15:18:56.

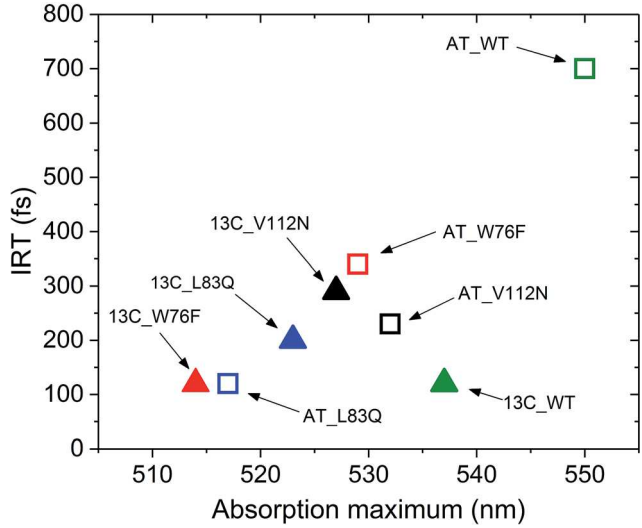

Fig. 10 Isomerization reaction times with respect to absorption maxima of AT (open squares) and 13C isomers (triangles) in wt-ASR and three mutants.

Interestingly, mutations with hydrophilic groups tend to slow down the IRT of the 13C isomer, while it significantly accelerates isomerization for the ATs (Table 3). For L83Q, the IRT of 13C is now slower than for AT, while the former is 7 times shorter than the latter in wt-ASR. Nevertheless, disregarding wt-ASR, the same trend as for AT is observed: a larger blue-shift of the absorption spectrum leads to a shorter IRT (Fig. 10).

Since the strongest effect of an enhanced IRT is observed for V112N, with a mutation in the vicinity of the ionone ring, *i.e.* far away from the C12=C13 double bond, the mechanism is most likely due to an electrostatic rather than a steric effect. Detailed excited state trajectory computations are needed, but the experimental results suggest that the 13C-PSBR excited state dipole moment increases during the reaction in a manner that reduces the slope of the S_1 PES, so as to slow down the excited state decay, with respect to the situation in wt-13C.

Conclusions and outlook

This paper reports the first detailed study on two aspects of the spectroscopy of Anabaena sensory rhodopsin, namely the vibrational spectra of the primary photoproducts K_{AT} and K_{13C} of wt-ASR and the effects of point mutations of ASR on the excited state decay and isomerization reaction times of the mutants V112N, W76F and L83Q. The ground state absorption spectra of these mutants are all blue-shifted with respect to wt-ASR and our quantum chemistry computations show that the electrostatic interactions in the PSBR binding pocket are responsible for the colour tuning in V112N and W76F. The transient absorption experiments show quite dramatic shortenings of the S_1 lifetimes and IRT's of the AT isomer with respect to wt-ASR. To the best of our knowledge, a 7-fold reduction of the excited state lifetime, as observed here for L83Q-AT is unique for a retinal protein, for which mutations generally induce slower and less efficient isomerization reactions. Such

Published on 15 November 2017. Downloaded by INIST - CNRS on 01/02/2018 15:18:56.

a slow-down is observed for the 13C. It is interesting to note that for AT, the shorter IRT's go along with the blue-shifted absorption spectra. Our strategy to proceed both experimentally and theoretically for providing a detailed comprehensive understanding of the mutation effects and of PSBR–protein interactions in general has made early progress, but it hinges presently on obtaining an adequate model for L83Q, and for realistic excited state trajectories for the three mutants. The time-resolved vibrational spectra will provide additional experimental data, to be tested by the QM/MM simulations.

The vibrational spectra of 13C and AT of wt-ASR, as well as the respective photoproducts, show all features well-known for bR and other rhodopsin systems in the region between 1000–1600 cm^{-1}. In particular, the separation of the 13C and AT contributions was demonstrated for the C=C and C–C stretching modes. The dephasing of the C=C for 13C is slower than for AT (1030 *vs.* 750 fs), hinting at a weaker coupling of this mode with the environment on the electronically ground state in respect to AT. Moreover, the frequency shifts detected and assigned for each isomer clearly show the potential of pump-DFWM to separate and resolve the small spectral changes due to mutation of ASR in the future.

Last, the specific biological function of ASR, as a photo-receptor for light-intensity level, requires differences in the absorption spectra of AT and CIS and differences in their isomerization quantum yield, so as to allow for sizeable changes of the isomer content upon light- or dark-adaptation. It will therefore be extremely important in the future to determine experimentally and understand theoretically the effect of the mutations on the reaction quantum yield.

Conflicts of interest

There are no conflicts to declare.

Acknowledgements

The Strasbourg team is grateful to Dr A. Cheminal for his contribution to the initial phase of the experiments, and to Dr O. Crégut and J.-P. Vola for technical assistance. The work was supported by the French-German ANR-DFG grant Femto-ASR (ANR-14-CE35-0015-01) and by the Labex NIE (ANR-11-LABX-0058_NIE). The France-Korea collaboration is supported by CNRS in the framework of the "LIA NanoFunc". M. O. is grateful for a USIAS 2015 Fellowship, and funding through the NSF Grant No. CHEM 1710191. D. A. thanks the "region Alsace" for partial funding of his PhD contract.

Notes and references

1 H. J. Polland, M. A. Franz, W. Zinth, W. Kaiser, E. Kölling and D. Oesterhelt, *Biophys. J.*, 1986, **49**, 651–662.
2 J. W. Petrich, J. Breton, J. L. Martin and A. Antonetti, *Chem. Phys. Lett.*, 1987, **137**, 369–375.
3 J. Herbst, K. Heyne and R. Diller, *Science*, 2002, **297**, 822–825.
4 R. Diller, in *Biological and Medical Physics, Biomedical Engineerin*, ed. M. Braun, P. Gilch and W. Zinth, Springer, Berlin Heidelberg, 2008, pp. 243–273.
5 J. Briand, J. Leonard and S. Haacke, *J. Opt.*, 2010, **12**, 084004.

 This journal is © The Royal Society of Chemistry 2018

Published on 15 November 2017. Downloaded by INIST - CNRS on 01/02/2018 15:18:56.

6 A. Wand, I. Gdor, J. Y. Zhu, M. Sheves and S. Ruhman, *Annu. Rev. Phys. Chem.*, 2013, **64**, 437–458.
7 I. Schapiro and S. Ruhman, *Biochim. Biophys. Acta, Bioenerg.*, 2014, **1837**, 589–597.
8 S. Ruhman, B. X. Hou, N. Friedman, M. Ottolenghi and M. Sheves, *J. Am. Chem. Soc.*, 2002, **124**, 8854–8858.
9 G. I. Groma, A. Colonna, J. C. Lambry, J. W. Petrich, G. Váró, M. Joffre, M. H. Vos and J.-L. Martin, *Proc. Natl. Acad. Sci. U. S. A.*, 2004, **101**, 7971–7975.
10 S. Schenkl, F. van Mourik, G. van der Zwan, S. Haacke and M. Chergui, *Science*, 2005, **309**, 917–920.
11 P. Kukura, D. W. McCamant, S. Yoon, D. B. Wandschneider and R. A. Mathies, *Science*, 2005, **310**, 1006–1009.
12 D. W. McCamant, P. Kukura and R. A. Mathies, *J. Phys. Chem. B*, 2005, **109**, 10449–10457.
13 J. P. Kraack, T. Buckup, N. Hampp and M. Motzkus, *ChemPhysChem*, 2011, **12**, 1851–1859.
14 J. P. Kraack, T. Buckup and M. Motzkus, *Phys. Chem. Chem. Phys.*, 2012, **14**, 13979–13988.
15 V. I. Prokhorenko, A. M. Nagy, S. A. Waschuk, L. S. Brown, R. R. Birge and R. J. D. Miller, *Science*, 2006, **313**, 1257–1261.
16 G. Vogt, P. Nuernberger, T. Brixner and G. Gerber, *Chem. Phys. Lett.*, 2006, **433**, 211–215.
17 P. J. M. Johnson, A. Halpin, T. Morizumi, V. I. Prokhorenko, O. P. Ernst and R. J. Dwayne Miller, *EPJ Web Conf.*, 2013, **41**, 07020.
18 D. Polli, P. Altoe, O. Weingart, K. M. Spillane, C. Manzoni, D. Brida, G. Tomasello, G. Orlandi, P. Kukura, R. A. Mathies, M. Garavelli and G. Cerullo, *Nature*, 2010, **467**, 440–U488.
19 T. Sovdat, G. Bassolino, M. Liebel, C. Schnedermann, S. P. Fletcher and P. Kukura, *J. Am. Chem. Soc.*, 2012, **134**, 8318–8320.
20 L. M. Frutos, T. Andruniow, F. Santoro, N. Ferre and M. Olivucci, *Proc. Natl. Acad. Sci. U. S. A.*, 2007, **104**, 7764–7769.
21 T. Andruniów, N. Ferré and M. Olivucci, *Proc. Natl. Acad. Sci. U. S. A.*, 2004, **101**, 17908–17913.
22 M. Ben-Nun, F. Molnar, K. Schulten and T. J. Martínez, *Proc. Natl. Acad. Sci. U. S. A.*, 2002, **99**, 1769–1773.
23 F. Molnar, M. Ben-Nun, T. J. Martínez and K. Schulten, *J. Mol. Struct.*, 2000, **506**, 169–178.
24 A. Cembran, F. Bernardi, M. Olivucci and M. Garavelli, *Proc. Natl. Acad. Sci. U. S. A.*, 2005, **102**, 6255–6260.
25 I. Schapiro, M. N. Ryazantsev, L. M. Frutos, N. Ferre, R. Lindh and M. Olivucci, *J. Am. Chem. Soc.*, 2011, **133**, 3354–3364.
26 I. Rivalta, A. Nenov, O. Weingart, G. Cerullo, M. Garavelli and S. Mukamel, *J. Phys. Chem. B*, 2014, **118**, 8396–8405.
27 P. Hamm, M. Zurek, T. Röschinger, H. Patzelt, D. Oesterhelt and W. Zinth, *Chem. Phys. Lett.*, 1996, **263**, 613–621.
28 S. L. Logunov, M. A. ElSayed, L. Song and J. K. Lanyi, *J. Phys. Chem.*, 1996, **100**, 2391–2398.
29 O. Bismuth, N. Friedman, M. Sheves and S. Ruhman, *J. Phys. Chem. B*, 2007, **111**, 2327–2334.

Published on 15 November 2017. Downloaded by INIST - CNRS on 01/02/2018 15:18:56.

30 O. Bismuth, N. Friedman, M. Sheves and S. Ruhman, *Chem. Phys.*, 2007, **341**, 267–275.
31 G. Zgrablić, S. Haacke and M. Chergui, *Chem. Phys.*, 2007, **338**, 168.
32 G. Zgrablic, S. Haacke and M. Chergui, *J. Phys. Chem. B*, 2009, **113**, 4384–4393.
33 G. Zgrablic, K. Voitchovsky, M. Kindermann, S. Haacke and M. Chergui, *Biophys. J.*, 2005, **88**, 2779–2788.
34 G. Bassolino, T. Sovdat, M. Liebel, C. Schnedermann, B. Odell, T. D. W. Claridge, P. Kukura and S. P. Fletcher, *J. Am. Chem. Soc.*, 2014, **136**, 2650–2658.
35 T. Ye, N. Friedman, Y. Gat, G. H. Atkinson, M. Sheves, M. Ottolenghi and S. Ruhman, *J. Phys. Chem.*, 1999, **103**, 5122.
36 S. Haacke, S. Schenkl, S. Vinzani and M. Chergui, *Biopolymers*, 2002, **67**, 306–309.
37 S. Haacke, S. Vinzani, S. Schenkl and M. Chergui, *ChemPhysChem*, 2001, **2**, 310–315.
38 G. Zgrablic, S. Haacke and M. Chergui, *J. Phys. Chem. B*, 2009, **113**, 4384–4393.
39 G. Zgrablić, A. M. Novello and F. Parmigiani, *J. Am. Chem. Soc.*, 2011, **134**, 955–961.
40 I. Burghardt and J. T. Hynes, *J. Phys. Chem. A*, 2006, **110**, 11411–11423.
41 L. Vogeley, O. A. Sineshchekov, V. D. Trivedi, J. Sasaki, J. L. Spudich and H. Luecke, *Science*, 2004, **306**, 1390–1393.
42 A. Kawanabe, Y. Furutani, K.-H. Jung and H. Kandori, *J. Am. Chem. Soc.*, 2007, **129**, 8644–8649.
43 A. Strambi, B. Durbeej, N. Ferré and M. Olivucci, *Proc. Natl. Acad. Sci. U. S. A.*, 2010, **107**, 21322–21326.
44 A. Wand, R. Rozin, T. Eliash, K.-H. Jung, M. Sheves and S. Ruhman, *J. Am. Chem. Soc.*, 2011, **133**, 20922–20932.
45 R. Rozin, A. Wand, K. H. Jung, S. Ruhman and M. Sheves, *J. Phys. Chem. B*, 2014, **118**, 8995–9006.
46 A. Wand, B. Loevsky, N. Friedman, M. Sheves and S. Ruhman, *J. Phys. Chem. B*, 2013, **117**, 4670–4679.
47 A. Cheminal, J. Leonard, S.-Y. Kim, K.-H. Jung, H. Kandori and S. Haacke, *Phys. Chem. Chem. Phys.*, 2015, **17**, 25429–25439.
48 A. Cheminal, J. Leonard, S. Y. Kim, K. H. Jung, H. Kandori and S. Haacke, *Chem. Phys. Lett.*, 2013, **587**, 75–80.
49 R. M. Weiss and A. W. Warshel, *J. Am. Chem. Soc.*, 1979, **101**, 6131–6133.
50 Y. Wada, A. Kawanabe, Y. Furutani, H. Kandori and H. Ohtani, *Chem. Phys. Lett.*, 2008, **453**, 105–108.
51 J. Briand, O. Braem, J. Rehault, J. Leonard, A. Cannizzo, M. Chergui, V. Zanirato, M. Olivucci, J. Helbing and S. Haacke, *Phys. Chem. Chem. Phys.*, 2010, **12**, 3178–3187.
52 J. Hauer, T. Buckup and M. Motzkus, *J. Phys. Chem. A*, 2007, **111**, 10517–10529.
53 J. P. Kraack, T. Buckup, N. Hampp and M. Motzkus, *Chem. Phys. Chem.*, 2011, **12**, 1851–1859.
54 T. Buckup and M. Motzkus, *Annu. Rev. Phys. Chem.*, 2015, **65**, 39–57.
55 F. Melaccio, M. Del Carmen Marin, A. Valentini, F. Montisci, S. Rinaldi, M. Cherubini, X. Yang, Y. Kato, M. Stenrup, Y. Orozco-Gonzalez, N. Ferre, H. L. Luk, H. Kandori and M. Olivucci, *J. Chem. Theory Comput.*, 2016, **12**, 6020–6034.

 This journal is © The Royal Society of Chemistry 2018

Published on 15 November 2017. Downloaded by INIST - CNRS on 01/02/2018 15:18:56.

56 A. Zen, E. Coccia, S. Gozem, M. Olivucci and L. Guidoni, *J. Chem. Theory Comput.*, 2015, **11**, 992–1005.
57 L. Andersen, I. Nielsen, M. Kristensen, M. El Ghazaly, S. Haacke, M. Nielsen and M. Petersen, *J. Am. Chem. Soc.*, 2005, **127**, 12347–12350.
58 R. A. Mathies, C. H. B. Cruz, W. T. Polard and C. V. Shank, *Science*, 1988, **240**, 777–779.
59 Q. Wang, R. W. Schoenlein, L. A. Peteanu, R. A. Mathies and C. V. Shank, *Science*, 1994, **266**, 422–424.
60 A. Kawanabe, Y. Furutani, K.-H. Jung and H. Kandori, *J. Am. Chem. Soc.*, 2007, **129**, 8644–8649.
61 A. Kawanabe and H. Kandori, *Sensors*, 2009, **9**, 9741–9804.
62 O. A. Smitienko, M. N. Mozgovaya, I. V. Shelaev, F. E. Gostev, T. B. Feldman, V. A. Nadtochenko, O. M. Sarkisov and M. A. Ostrovsky, *Biochemistry*, 2009, **75**, 34–45.
63 A. V. Sharkov, A. V. Pakulev, S. V. Chekalin and a. Y. A. Matveetz, *Biochim. Biophys. Acta*, 1985, **808**, 94–102.
64 J. P. Kraack, T. Buckup and M. Motzkus, *Phys. Chem. Chem. Phys.*, 2011, **13**, 21402–21410.
65 J. P. Kraack, T. Buckup and M. Motzkus, *Phys. Chem. Chem. Phys.*, 2012, **14**, 13979–13988.
66 J. P. Kraack, T. Buckup and M. Motzkus, *J. Phys. Chem. Lett.*, 2013, **4**, 383–387.
67 J. P. Kraack, A. Wand, T. Buckup, M. Motzkus and S. Ruhman, *Phys. Chem. Chem. Phys.*, 2013, **15**, 14487–14501.
68 M. S. Marek, T. Buckup and M. Motzkus, *J. Phys. Chem. B*, 2011, **115**, 8328–8337.
69 T. Miki, T. Buckup, M. S. Krause, J. Southall, R. J. Cogdell and M. Motzkus, *Phys. Chem. Chem. Phys.*, 2016, **18**, 11443–11453.
70 S. Fujiyoshi, S. Takeuchi and T. Tahara, *J. Phys. Chem. A*, 2003, **107**, 494–500.
71 M. Liebel and P. Kukura, *J. Phys. Chem. Lett.*, 2013, **4**, 1358–1364.
72 M. Liebel, C. Schnedermann and P. Kukura, *Phys. Rev. Lett.*, 2014, **112**, 198302.
73 C. Schnedermann, V. Muders, D. Ehrenberg, R. Schlesinger, P. Kukura and J. Heberle, *J. Am. Chem. Soc.*, 2016, **138**, 4757–4762.
74 A. Kahan, O. Nahmias, N. Friedman, M. Sheves and S. Ruhman, *J. Am. Chem. Soc.*, 2007, **129**, 537–546.
75 P. Kukura, D. W. McCamant, S. Yoon, D. B. Wandschneider and R. A. Mathies, *Science*, 2005, **310**, 1006–1009.
76 P. Kukura, D. W. McCamant and R. A. Mathies, *Annu. Rev. Phys. Chem.*, 2007, **58**, 461–488.
77 I. Schapiro, *J. Phys. Chem. A*, 2016, **120**, 3353–3365.
78 S. Shim, J. Dasgupta and R. A. Mathies, *J. Am. Chem. Soc.*, 2009, **131**, 7592–7597.
79 M. Braiman and R. Mathies, *Proc. Natl. Acad. Sci. U. S. A.*, 1982, **79**, 403–407.
80 S. Smith, J. A. Pardoen, J. Lugtenburg and R. A. Mathies, *J. Phys. Chem.*, 1987, **91**, 804–819.
81 S. Rinaldi, F. Melaccio, S. Gozem, F. Fanelli and M. Olivucci, *Proc. Natl. Acad. Sci. U. S. A.*, 2014, **111**, 1714–1719.
82 Y. Orozco-Gonzalez, M. Manathunga, M. del Carmen Marín, D. Agathangelou, K.-H. Jung, F. Melaccio, N. Ferré, S. Haacke, K. Coutinho, S. Canuto and M. Olivucci, *J. Chem. Theory Comput.*, 2017, **13**, 6391–6404.